Applied Thermal Engineering 113 (2017) 1547–1557

Contents lists available at ScienceDirect

Applied Thermal Engineering

journal homepage: www.elsevier.com/locate/apthermeng

Research Paper

Heat transfer correlations for single-phase flow in plate heat exchangers based on experimental data

Jie Yang [a,b], Anthony Jacobi [b,*], Wei Liu [a]

[a] School of Energy and Power Engineering, Huazhong University of Science and Technology, Wuhan 430074, China
[b] Mechanical Science and Engineering, University of Illinois, Urbana 61801, IL, USA

HIGHLIGHTS

- Single-phase heat transfer performance for plate heat exchangers is investigated.
- High Prandtl number fluid is used as the working fluid.
- Various empirical correlations are provided based on experimental data.
- A generalized correlation is proposed based experimental and archival data.

ARTICLE INFO

Article history:
Received 22 June 2016
Revised 10 September 2016
Accepted 22 October 2016
Available online 16 November 2016

Keywords:
Brazed-plate heat exchanger
Single-phase heat transfer
Correlation
Performance

ABSTRACT

In the present paper, the single-phase heat transfer for nine brazed-plate heat exchangers with different geometric parameters is experimentally investigated. An ethylene glycol and water mixture is used as working fluid. First, the results show that the herringbone angle is the most dominant factor influencing heat transfer. Then, the results also show that geometric dimensions affect heat transfer jointly with herringbone angle. Individual correlations and a general correlation based on experimental data are presented. Then the empirical equations are compared to existing correlations from the open literature. Based on archival data and the experimental data presented in this work, a generalization of single-phase heat transfer performance of plate heat exchangers is given, relating the Nusselt number to heat exchanger geometry, Reynolds number, and fluid properties. The proposed correlation is based on experiments of 22 heat exchangers and 25 empirical correlations, and the percent root-mean-square deviation is 20.77%. This novel correlation has the accuracy of 50% and it is applicable for a very large range of plate heat exchangers.

1. Introduction

According to Thulukkanam [1], the plate heat exchanger (PHE) was invented by Richard Seligman in 1923. In early applications, plate heat exchangers (PHEs) were utilized for hygienic reasons in the fields such as the dairy and paper/pulp industries [2]. Later they found broader application in heating, ventilation, and air-conditioning systems [2]. Again according to Thulukkanam [1], in the 1990s the brazed plate heat exchanger (BPHE) was invented. Adjacent plates are welded, brazed, or soldered together to form inner flow channels, instead of being sealed by gaskets. As with the PHE, the BPHE provides excellent thermal-hydraulic performance, low-charge charge operation, and its highly compactness; moreover, the BPHE is capable of withstanding high pressure. The disadvantage of the BPHE compared with the PHE is that mechanically cleaning is much more difficult [1].

To date, both single-phase flow [2–27] and two-phase flow [2–4,28–36] in BPHEs have been studied. For single-phase flows, geometric parameters (such as chevron/herringbone angle, enlargement factor, and corrugation profile aspect ratio), working fluid, and flow maldistribution are three important factors that influence thermal-hydraulic characteristics. For two-phase flow, working conditions (such as vapor quality, mass flux, heat flux, and saturation temperature) also play significant roles in performance. Although much research have been completed over the past eighty years, there is still a dearth of design information available in the open literature like general heat transfer and pressure drop correlations, due to the proprietary nature of the PHE industry. Many results are important but applicable for very limited

* Corresponding author.
E-mail address: a-jacobi@illinois.edu (A. Jacobi).

http://dx.doi.org/10.1016/j.applthermaleng.2016.10.147
1359-4311/

Nomenclature

A_{proj}	projected heat transfer area (m^2)
A_{real}	real heat transfer area (m^2)
ACRC	Air Conditioning and Refrigeration Center (–)
b	corrugation depth (m)
BPHE	brazed plate heat exchanger (–)
c	specific heat ($J\,kg^{-1}\,K^{-1}$)
C_1, C_2	constants in Eq. (4)
D_h	hydraulic diameter (m) ($2b$)
EBD	the energy balance deviation (–)
EG	ethylene glycol (–)
h	heat transfer coefficient ($W\,m^{-2}\,K^{-1}$)
k	thermal conductivity ($W\,m^{-1}\,K^{-1}$)
L_1, L_2	plate length in Fig. 1 (m)
m	mass flow rate ($kg\,s^{-1}$)
n	channel number for the corresponding side (–)
Nu	Nusselt number (–) ($Nu = hD_h/k$)
PHE	plate heat exchanger (–)
Pr	Prandtl number (–) ($Pr = c\mu/k$)
Q	heat transfer rate (W)
Re	Reynolds number (–) ($Re = \rho VD_h/\mu$)
RTD	resistance temperature detector (–)
t	plate thickness (m)
T	temperature (K)
U	overall heat transfer coefficient ($W\,m^{-2}\,K^{-1}$)
V	fluid velocity in BPHE (m/s) ($V = m/(\rho nW_1 b)$)
W_1, W_2	plate width in Fig. 1 (m)

Greek symbols

β	herringbone angle (°)
γ	corrugation profile aspect ratio (–) ($\gamma = 2b/\lambda$)
λ	corrugation pitch in Fig. 1 (m)
ϕ	enlargement factor (–) ($\phi = A_{real}/A_{proj}$)
μ	dynamic viscosity
ΔT_{LMTD}	the counter-flow log-mean temperature difference (°C)

Subscripts

ave	average value
c	cold-side
h	hot-side
i	inlet
o	outlet
w	wall

geometry, fluid, or operating conditions. There has been some work in which researchers focus on the generalization, using a theoretical approach, model predictions and empirical correlations, for design and optimization [12,2,20,23]. However, the current design tools remain restricted, even for single-phase flows; the situation for two-phase flow is even less complete.

There are a number of archival publications about heat transfer with high-Prandtl-number fluids in BPHEs, which is of importance in the petrochemical and food-processing industries [6,16,17,22]. In 1964, Jackson and Troupe [6] developed a heat transfer correlation for laminar flow in a PHE using water and corn syrup as working fluids. In 1995, Talik et al. [16] explored single-phase flow in a PHE using a propylene glycol-water mixture ($70 < Pr < 450$) as the working fluid. Muley and Manglik [17] later conducted experiments with three PHEs, and used vegetable oil ($130 < Pr < 290$) as testing fluid. They developed empirical correlations to calculate the Nusselt number and friction coefficient and found that their correlations lack general applicability. More recently, Hayes and Jokar [22] used a dynalene/water mixture as cooling fluid for CO_2 condensation in a BPHE due to its lower viscosity compared to that of a ethylene glycol/water mixture. They found that the heat transfer performance depended on fluid properties, with viscosity especially relevant, even for the same BPHE. Therefore, empirical thermal-hydraulic correlations for high-Prandtl-number fluids may require development separately from work with low-Prandtl-number fluids.

In each of the articles discussed above on high-Prandtl-number flows in PHEs, a specific correlation for a certain PHE is given, and the same "custom" approach prevails for low-viscosity fluids. There is little general information, because each study is limited to a particular PHE geometry, fluids, and operating conditions. Therefore more experimental data with broader range of geometric parameters, fluids, and working conditions is needed if more general correlations for the Nusselt number and friction factor are to be developed. Moreover, even with more extensive data, the degree to which generalization can be achieved is unclear. In the present paper, an experimental investigation of single-phase heat transfer is presented for nine different BPHEs. An ethylene glycol (EG) and water mixture ($50 \leqslant Pr \leqslant 150$) is used as the working fluid. Specific correlations are proposed for different heat exchangers, and experimental data are obtained to fill gaps in the open literature, thus laying a foundation for heat transfer generalization. Finally, generalized correlations based on new experimental data and archival data from the literature are proposed.

2. Experiment

2.1. Experimental apparatus

Schematic diagrams of a typical BPHE and the experimental apparatus are shown in Figs. 1 and 2, respectively. The experimental apparatus consists of three loops, which are the hot-side loop, the cold-side loop, and the chiller loop. The hot-side loop contains a 6 kW electrical heater, an EG/water (65 vol%) tank, a pump, a

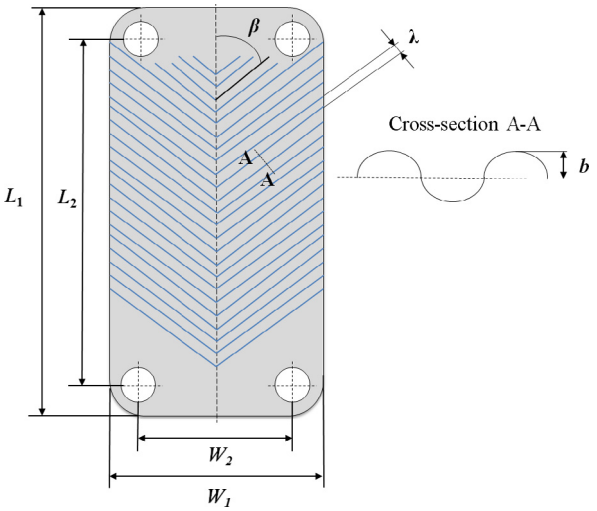

Fig. 1. The schematic diagram of plate heat exchanger.

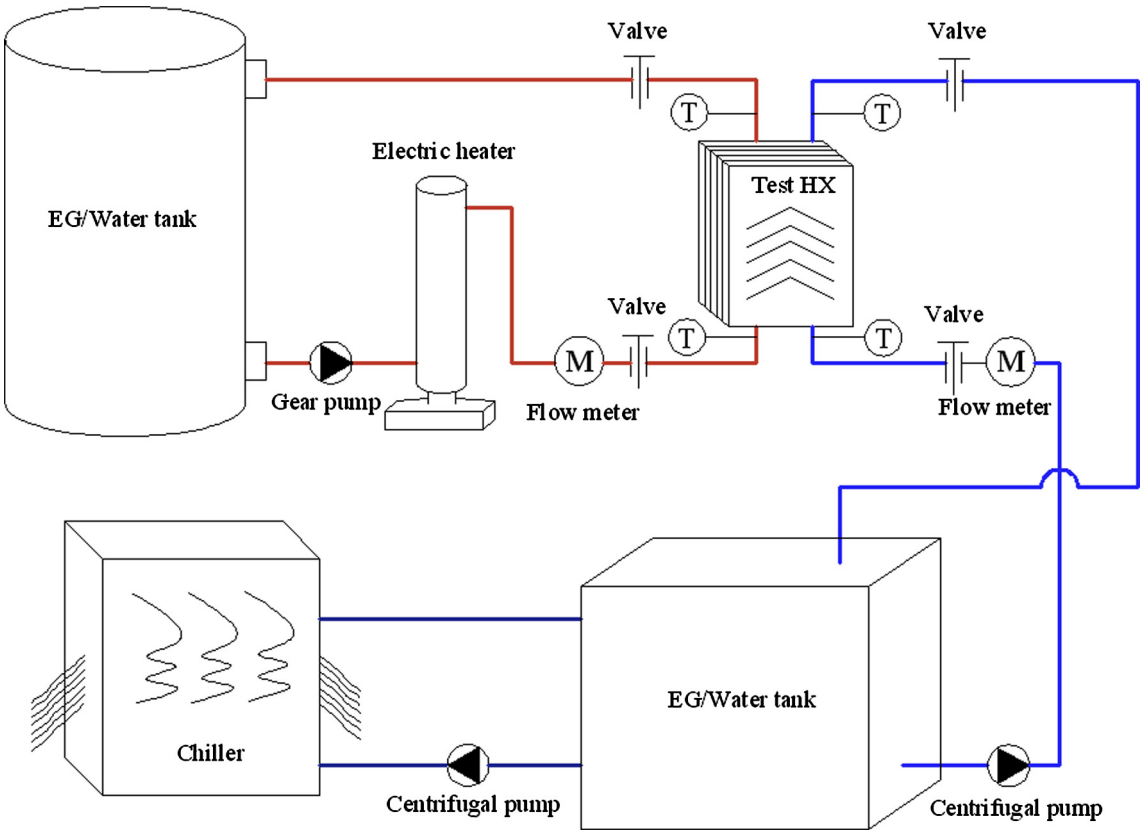

Fig. 2. The schematic diagram of experimental apparatus.

mass flow meter and one side of a test BPHE. The cold-side loop contains the other side of the test BPHE, a pump, a mass flow meter, and another EG/water (65 vol%) tank. The chiller loop contains a 20 kW chiller and a pump, and uses the same EG/water mixture tank of the cold-side loop. When the experiment is in steady operation, the heat generated by electrical heater is transferred from the hot-side to the cold-side loop in the test BPHE, and it is ultimately from the cold-side loop to building water by the chiller.

The mass flow rates for the hot-side and the cold-side are measured using two Coriolis-effect flow meters with a precision of 0.05% of the reading. The fluid temperature is measured using four RTD sensors with the precision ranging from 0.03 K to 0.05 K depending on the measured temperature. The four sensors are inserted at the hot-side inlet, hot-side outlet, cold-side inlet, and cold-side outlet of the test BPHE. All temperature and flow rate data are automatically recorded using a data acquisition system. The mass flow rates range from 0.0378 kg/s to 0.378 kg/s. The temperature for the hot-side inlet, hot-side outlet, cold-side inlet, and cold-side outlet ranges from 25 to 35 °C, from 20 to 30 °C, from 0 to 10 °C, and from 5 to 15 °C, respectively.

The geometric parameters for the test BPHEs are given in Table 1. ϕ is the enlargement factor, which is the ratio of the real area to the projected area; while γ is the corrugation profile aspect ratio ($\gamma = 2b/\lambda$). It should be noted that BPHE #1, #2, #5, #6, and #7 are assembled using plates with the same herringbone angle of 65°, and BPHE #4 and #9 are assembled using plates with identical herringbone angle of 27°. As for BPHE #3 and #8, one flow channel is created by using plates with different herringbone angles, β is 65° for one plate and 27° for the other. Hence, the herringbone angle for BPHE #3 and #8 is taken as 46°, the average of 65° and 27°. All thermal physical parameters for EG/water mixture such as density, thermal conductivity, viscosity, and specific heat are evaluated at the average bulk temperature for the corresponding side. All parameters for stainless steel are evaluated at the average temperature of hot-side and cold-side. The heat transfer from the hot-side is compared to that transferred to the cold-side, with each measurement recorded when the experiment is in steady operation (the temperature fluctuates within 0.4 °C in 2 h) for twenty minutes. The EBD (energy balance deviation) between hot-side and cold-side is defined as follows:

$$EBD = \frac{|Q_h - Q_c|}{Q_{ave}} \times 100\% \quad (1)$$

where Q_h and Q_c are the heat transfer power for hot-side and cold-side, and Q_{ave} is the average value of Q_h and Q_c. The energy balance deviation for 119 measurements for all BPHEs is shown in Fig. 3, where 95% of the measurements have an energy balance within 3.9%.

2.2. Data reduction

As the uncertainties of Q_h and Q_c are very close, the heat transfer power Q is therefore calculated as follows for simplicity:

$$Q = \frac{m_h \cdot c_h(T_{h,i} - T_{h,o}) + m_c \cdot c_c(T_{c,o} - T_{c,i})}{2} \quad (2)$$

where m is the mass flow rate, c is the specific heat, T is the temperature. It should be noted that the arithmetic mean heat transfer is not preferred if the experimental uncertainties for two sides are not identical, as Park et al. suggested in [37]. The overall heat transfer coefficient U is calculated as follows:

Table 1
The geometric parameters of BPHEs.

BPHE	#1	#2	#3	#4	#5	#6	#7	#8	#9
L_1 (mm)	527	527	527	527	325	325	207	207	207
L_2 (mm)	466	466	466	466	269	269	172	172	172
W_1 (mm)	111	111	111	111	95	95	77	77	77
W_2 (mm)	50	50	50	50	39	39	42	42	42
β (°)	65	65	46.5	27	65	65	65	46.5	27
b (mm)	2	2	2	2	1.25	1.25	2	2	2
λ (mm)	7	7	7	7	4	4	7	7	7
t (mm)	0.4	0.4	0.4	0.4	0.3	0.3	0.3	0.3	0.3
ϕ	1.16	1.16	1.16	1.16	1.18	1.18	1.16	1.16	1.16
γ	0.571	0.571	0.571	0.571	0.625	0.625	0.571	0.571	0.571
Plate no.	10	10	10	10	10	10	10	10	10
Distributor	Yes	No	No	No	Yes	No	No	No	No

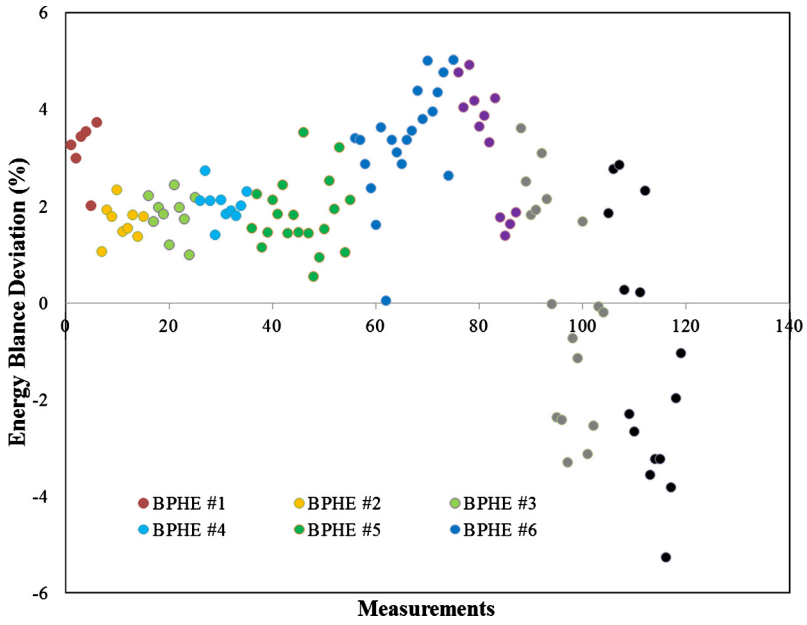

Fig. 3. Energy balance deviation for all measurements.

$$U = \frac{Q}{A_{proj} \cdot \Delta T_{LMTD}} \tag{3}$$

where A_{proj} is the projected heat transfer area, $L_2 \times W_1$, (also sometimes referred to as the nominal heat transfer area), and ΔT_{LMTD} is the counter-flow log-mean temperature difference. In order to develop a heat transfer correlation for single-phase flow, the modified Wilson plot technique is adopted [38]. Assuming the correlations for both hot-side and cold-side can be written as follows, with appropriate values for C_1 and C_2 [39]:

$$Nu = C_1 Re^{C_2} Pr^{\frac{1}{3}} \left(\frac{\mu}{\mu_w}\right)^{0.14} \tag{4}$$

Further assuming the correlation for the hot-side is identical to the correlation for the cold-side for one BPHE, both the hot-side and the cold-side flows have the same values for the constants C_1 and C_2. Neglecting fouling effects, the thermal resistance of the hot-side flow can be expressed as follows:

$$\frac{1}{A_{proj} \cdot h_h} = \frac{1}{A_{proj} \cdot U} - \frac{t}{A_{proj} \cdot k_w} - \frac{1}{A_{proj} \cdot h_c} \tag{5}$$

where t is the plate thickness, and k_w is thermal conductivity of the plate. Then substituting Eqs. (4) into (5) and using the definition of Nu:

$$\left(\frac{1}{U} - \frac{t}{k_w}\right)\left\{Re_c^{C_2} Pr_c^{1/3}\left(\frac{k_c}{D_h}\right)\left(\frac{\mu}{\mu_w}\right)_c^{0.14}\right\} = \frac{1}{C_1} + \left(\frac{1}{C_1}\right)\left\{\left(\frac{Re_c}{Re_h}\right)^{C_2}\left(\frac{Pr_c}{Pr_h}\right)^{1/3}\left(\frac{k_c}{k_h}\right)\left(\frac{\mu_c \mu_{w,h}}{\mu_h \mu_{w,c}}\right)^{0.14}\right\} \tag{6}$$

where D_h is hydraulic diameter. In the present work, the hydraulic diameter is defined as suggested in [40]:

$$D_h = 2b \tag{7}$$

where b is the corrugation depth, as shown in Fig. 1. The Reynolds number is defined as:

$$Re = \frac{\rho V D_h}{\mu} \tag{8}$$

where ρ is density, V is the velocity inside a BPHE defined in the following form:

$$V = \frac{m}{\rho n W_1 b} \tag{9}$$

where n is the channel number for the corresponding side. With the measured temperatures, measured flow rates, known heat exchanger dimensions and thermo-physical properties, the average plate wall temperatures are calculated as part of determining the curve

parameters C_1 and C_2 using the following equations in an iterative scheme as described below:

$$Q = h_h \cdot A_{proj}(T_{ave,h} - T_{w,h}) \tag{10a}$$

$$Q = h_c \cdot A_{proj}(T_{ave,c} - T_{w,c}) \tag{10b}$$

$$Q = k_w \cdot A_{proj}/t(T_{w,h} - T_{w,c}) \tag{10c}$$

Eq. (6) can be written as:

$$YY = \frac{1}{C_1}XX + \frac{1}{C_1} \tag{11}$$

where

$$YY = \left(\frac{1}{U} - \frac{t}{k_w}\right)\left\{Re_c^{C_2} Pr_c^{1/3}\left(\frac{k_c}{D_h}\right)\left(\frac{\mu}{\mu_w}\right)_c^{0.14}\right\} \tag{12}$$

$$XX = \left(\frac{Re_c}{Re_h}\right)^{C_2}\left(\frac{Pr_c}{Pr_h}\right)^{1/3}\left(\frac{k_c}{k_h}\right)\left(\frac{\mu_c\mu_{w,h}}{\mu_h\mu_{w,c}}\right)^{0.14} \tag{13}$$

In Eq. (12), YY depends on $\mu_{w,c}$, which is evaluated at $T_{w,c}$; likewise XX in Eq. (12), depends on the wall temperatures due to properties evaluations. The solution is undertaken by guessing a value for $T_{w,h}$, and then $T_{w,c}$ is calculated with Eq. (10c). With these temperatures available, the coefficient C_1 and the exponent C_2 on Reynolds number are obtained by minimizing the least-squared error of the experimental data with respect to Eq. (11). Now, with C_1 and C_2 available, Eq. (4) and the definition of the Nusselt number are used with Eq. (10a) to calculate $T_{w,h}$. This value is taken as the new guess to restart the calculation, and the process continues iteratively until the change in $T_{w,h}$ is less than its experimental uncertainty. Once convergence is achieved for $T_{w,h}$ it is held fixed, and using Eq. (10c) a value is calculated for $T_{w,c}$, allowing C_1 and C_2 to be determined anew by least-squared error. With convergence on $T_{w,h}$ and $T_{w,c}$, Eq. (10b) is used to re-check that Q is within its experimental uncertainty. For example, the modified Wilson plot for #2 is presented as in Fig. 4. It should be noted that the modified Wilson plot can be utilized to build the empirical correlations for #2, #3, #4, #6, #7, #8, and #9. But for #1 and #5, there are distributors in cold-side so the assumption that hot-side and cold-side correlations are identical might not be valid. Therefore, the modified Wilson plot was not utilized for #1 and #5; instead, the following procedure was adopted. Since the hot-side is the same for #1 and #2, the hot-side correlation for #2 is used for the hot-side for #1. Thus, the cold-side correlation for #1 can be calculated from the data for the overall heat transfer coefficient for #1 and hot-side correlation for #2. The same method applies for #5. Therefore the cold-side correlations with distributors for #1 and #5 are established. The empirical correlations are presented in Table 2. Calculated value of experimentally measured U versus U obtained using the correlations in Table 2 is presented in Fig. 5.

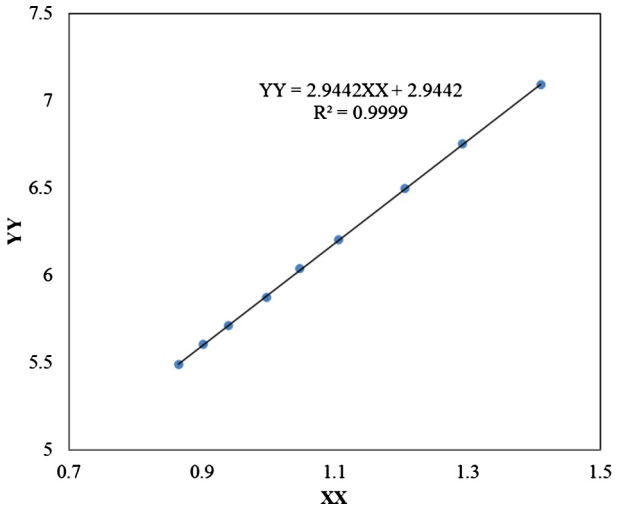

Fig. 4. The modified Wilson plot for BPHE #2.

2.3. Uncertainty in experimental data

The uncertainties of the experimental data are calculated using standard methods [41,42]. The uncertainties for temperature, flow rate, Reynold number, Nusselt number, and overall heat transfer coefficient are shown in Table 3.

2.4. The distributor effect

The heat transfer correlations for #1, #2, #5, and #6 are plotted in Fig. 6, where it can be seen that the difference between #1 and # 2 is less than 1% for the entire Re range. The difference between #5 and #6 is less than 1% as well for all Re. It is therefore concluded that for large and medium plate heat exchangers with a high herringbone angle, the single-phase flow is well-distributed. For single-phase flow, installing distributors does not enhance heat transfer, but it will increase pressure drop and thus pumping power.

2.5. The geometry effect

The empirical heat transfer correlations for #2, #3, #4, #6, #7, #8, and #9 are plotted for comparison in Fig. 7. It is demonstrated that among all geometric parameters, the herringbone angle is the most influential factor on the heat transfer characteristics. It is also apparent that geometric dimensions ($L \times W$) have an impact on heat transfer. At a low herringbone angle, the large BPHE has a better heat transfer performance than the small one when Re is below 200. The small BPHE displays a better performance when Re exceeds 200. At a medium herringbone angle, the heat transfer deviation between the large and the small BPHEs is from 8.7% to 1.1% as the Re ranges from 50 to 500. At a high herringbone angle, the medium BPHE demonstrates the best heat transfer performance, while the small BPHE has the worst heat transfer performance. Overall, geometric dimensions have less impact on heat transfer performance than does the herringbone angle. From the curves for #2, #6, and #7, it is also concluded that when herringbone angle is the same, the BPHE with the largest corrugation profile aspect ratio has the best heat transfer performance, which is consistent with results in literature.

Based on our experimental data for nine different heat exchangers, an empirical correlation is given to predict the single-phase heat transfer performance in plate heat exchanger for $50 \leqslant Pr \leqslant 150$:

Table 2
The experimental correlations of tested brazed plate heat exchangers.

BPHE number	$Nu/(Pr^{1/3}(\mu/\mu_w)^{0.14})$
#1	$0.341Re^{0.721}$
#2	$0.340Re^{0.721}$
#3	$0.164Re^{0.755}$
#4	$0.355Re^{0.554}$
#5	$0.248Re^{0.785}$
#6	$0.247Re^{0.785}$
#7	$0.341Re^{0.710}$
#8	$0.214Re^{0.714}$
#9	$0.155Re^{0.695}$

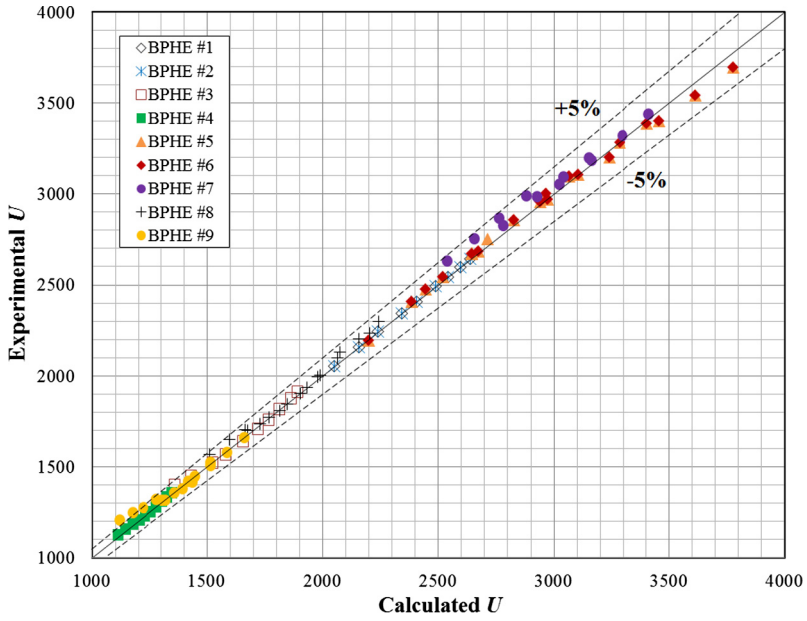

Fig. 5. Calculated value of experimentally measured U versus U obtained using the correlations in Table 2.

Table 3
The uncertainty of experiment.

Parameters	Uncertainty
Temperature	0.03–0.05 K
Flow rate	0.05%
Reynolds number	0.05%
Nusselt number	5.35–5.73%
Overall heat transfer coefficient	5.27–5.79%

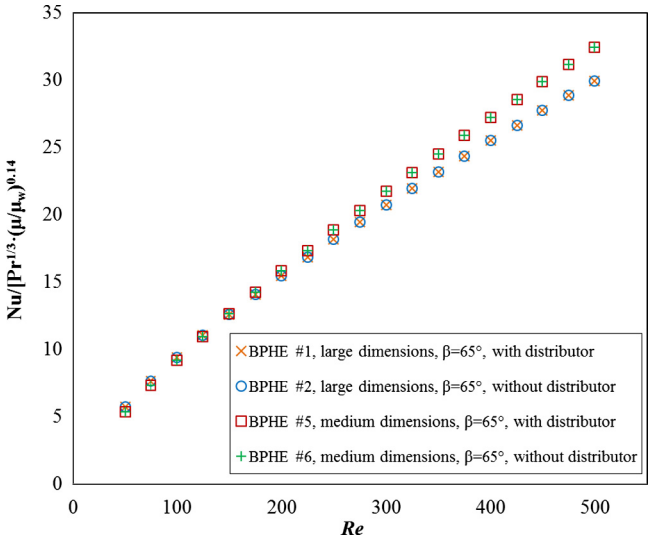

Fig. 6. The distributor effect on single-phase heat transfer.

$$Nu = \left(4.669\times10^{-5}\cdot\beta^2 - 2.009\times10^{-3}\cdot\beta + 0.1067\right) \cdot Re^{\left(-2.286\times10^{-5}\cdot\beta^2+2.921\times10^{-3}\cdot\beta+0.6477\right)} \cdot Pr^{1/3} \cdot \left(\frac{\mu}{\mu_w}\right)^{0.14}$$
$$50 \leqslant Re \leqslant 500;\ \ 50 \leqslant Pr \leqslant 150 \qquad (14)$$

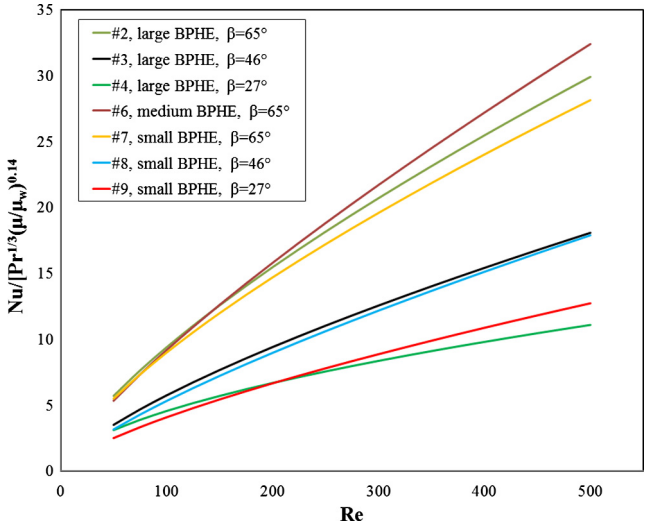

Fig. 7. The heat transfer characteristics for different BPHEs with different geometric parameters.

The heat transfer performance calculated using Eq. (14) is plotted with the experimental heat transfer performance for comparison in Fig. 8. It is clear that Eq. (14) provides accurate predictions of the heat transfer in this Prandtl number range, with 95% of the data within 8.5%, and all data within 10%.

2.6. Generalization based on experimental data

The existing correlations from the literature [8,15,17,18,29,33,36], listed in Table 4, were selected for comparison to the current work. It should be noted that for different empirical correlations, the definitions of heat transfer area (A) and hydraulic diameter (D_h) differ. A comparison is valid only when all parameters are defined in the same way. Since the projected heat transfer area is used to calculate U in the present work, all correlations using the actual heat transfer area ($\phi \times A_{proj}$) need

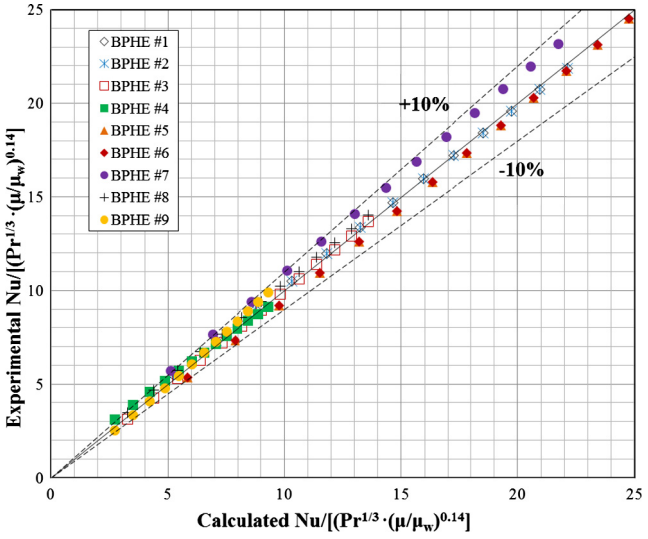

Fig. 8. Heat transfer characteristics obtained using Eq. (14) versus the experimental heat transfer characteristics.

to be modified for a valid comparison. The modification procedure is conducted through the following procedure:

$$R_{overall} = \frac{A_{\text{real}} \cdot \Delta T_{LMTD}}{Q} \tag{15a}$$

$$R_{overall} = \frac{\phi A_{\text{proj}} \cdot \Delta T_{LMTD}}{Q} \tag{15b}$$

$$R_{overall} = \frac{t}{k_w} + \frac{D_h}{k_c \cdot C_1 Re_c^{C_2} Pr_c^{1/3} (\mu/\mu_w)_c^{0.14}} + \frac{D_h}{k_h \cdot C_1 Re_h^{C_2} Pr_h^{1/3} (\mu/\mu_w)_h^{0.14}} \tag{15c}$$

The thermal resistance of wall conduction can be ignored as the convective thermal resistance is two or three orders of magnitude larger, depending on flow conditions. Therefore Eq. (15) can be written as:

$$\frac{R_{overall}}{\phi} = \frac{A_{proj} \cdot \Delta T_{LMTD}}{Q} \tag{16a}$$

Table 4
Some exsiting correlations in chronological order.

Year	Author	A	D_h	Application range
1985	Fcoke et al.[8]	A_{proj}	$2b$	$27 \leqslant Re \leqslant 56{,}000$
$Nu = C_1 Re^{C_2} Pr^{0.5}$				
β		Re	C_1	C_2
0°		8000–56,000	0.021	0.868
30°		120–1000	0.77	0.54
		1000–42,000	0.44	0.64
45°		45–300	1.67	0.44
		300–2000	0.405	0.7
		2000–20,000	0.84	0.6
60°		20–150	1.89	0.46
		150–600	0.57	0.7
		600–16,000	1.112	0.6
72°		200–4000	1.45	0.58
80°		27–500	1.05	0.64
		500–2800	1.98	0.54
90°		300–14,000	0.98	0.63
1995	Talik et al. [15]	A_{proj}	$2b$	$1450 \leqslant Re \leqslant 11{,}460$; $2.5 \leqslant Pr \leqslant 5.0$
$Nu = 0.248 Re^{0.7} Pr^{0.4}$				
1999	Muley and Manglik [17]	A_{real}	$2b$	$1000 \leqslant Re$; $2 \leqslant Pr \leqslant 6$
$Nu = \left(0.2668 - 6.967 \times 10^{-3} \cdot \beta + 7.244 \times 10^{-5} \times \beta^2\right) \cdot Re^{[0.728 + 0.0543 \sin\left(\frac{\pi\beta}{45} + 3.7\right)]} Pr^{0.333} \left(\frac{\mu}{\mu_w}\right)^{0.14}$				
1999	Muley et al.[18]	A_{real}	$2b$	$30 \leqslant Re \leqslant 400$; $130 \leqslant Pr \leqslant 290$
$Nu = 1.6774 (d_e/L)^{1/3} (\beta/30)^{0.38} Re^{0.5} Pr^{0.333} \left(\frac{\mu}{\mu_w}\right)^{0.14}$				
2003	Han et al.[29]	A_{real}	$2b/\phi$	$2000 \leqslant Re$; $2 \leqslant Pr \leqslant 6$
$Nu = 0.295 (\beta)^{0.09} Re^{0.64} Pr^{0.32}$				
2009	Hayes et al.[33]	A_{real}	$2b$	$400 \leqslant Re \leqslant 1000$; $15 \leqslant Pr \leqslant 50$
$Nu = C_1 Re^{C_2} Pr^{0.333} \left(\frac{\mu}{\mu_w}\right)^{0.14}$				
β		Re	C_1	C_2
30°		$400 \leqslant Re \leqslant 1000$	0.177	0.744
46.5°		$400 \leqslant Re \leqslant 700$	0.278	0.745
63°		$400 \leqslant Re \leqslant 700$	0.561	0.726
2009	Hayes et al. [33]	A_{real}	$2b$	$2000 \leqslant Re \leqslant 8000$; $2 \leqslant Pr \leqslant 6$
$Nu = C_1 Re^{C_2} Pr^{0.333} \left(\frac{\mu}{\mu_w}\right)^{0.14}$				
β		Re	C_1	C_2
30°		$2000 \leqslant Re \leqslant 8000$	0.134	0.712
46.5°		$2000 \leqslant Re \leqslant 7000$	0.214	0.698
63°		$2000 \leqslant Re \leqslant 4500$	0.240	0.724
2010	Khan et al.[36]	A_{real}	$2b/\phi$	$500 \leqslant Re \leqslant 2500$; $3.5 \leqslant Pr \leqslant 6.5$
$Nu = \left(0.0161 \frac{\beta}{\beta_{\max}} + 0.1298\right) Re^{\left(0.198 \frac{\beta}{\beta_{\max}} + 0.6398\right)} Pr^{0.35} \left(\frac{\mu}{\mu_w}\right)^{0.14}$				

$$\frac{R_{overall}}{\phi} = \frac{D_h}{k_c \cdot \phi \cdot C_1 Re_c^{C_2} Pr_c^{1/3} (\mu/\mu_w)_c^{0.14}} + \frac{D_h}{k_h \cdot \phi \cdot C_1 Re_h^{C_2} Pr_h^{1/3} (\mu/\mu_w)_h^{0.14}} \quad (16b)$$

So the correlations regarding A_{real} as heat transfer area can be easily modified into the correlations regarding A_{proj} as heat transfer area simply by multiplying the coefficient C_1 with enlargement factor ϕ. As for the correlations considering $2b/\phi$ as hydraulic diameter, they can be adjusted by the following procedure:

$$R_{con} = \frac{D_h}{C_1 \left(\frac{\rho v D_h}{\mu}\right)^{C_2} Pr^{0.333} (\mu/\mu_w)^{0.14} \cdot k} \quad (17a)$$

$$R_{con} = \frac{2b/\phi}{C_1 \left(\frac{\rho v 2b}{\mu\phi}\right)^{C_2} Pr^{0.333} (\mu/\mu_w)^{0.14} \cdot k} \quad (17b)$$

$$R_{con} = \frac{2b}{\phi^{1-C_2} \cdot C_1 \left(\frac{\rho v 2b}{\mu}\right)^{C_2} Pr^{0.333} (\mu/\mu_w)^{0.14} \cdot k} \quad (17c)$$

where R_{con} refers to convective heat transfer thermal resistance for either hot-side or cold-side. Therefore, correlations that take $2b/\phi$ as the hydraulic diameter can be simplified by multiplying the coefficient C_1 with the coefficient ϕ^{1-C_2}.

Finally, an attempt to generalize the correlations is undertaken. The presence of viscosity-variation correction factor $(\mu/\mu_w)^{0.14}$ has little effect for low viscous fluid (water, $Pr \sim 6$), but has a 3–20% impact for high viscous fluid (oil, $Pr \sim 290$) [18]. The current results indicate that the deviation is around 4% between the EG/water correlations with or without $(\mu/\mu_w)^{0.14}$ for high viscous fluid (EG/water, $Pr \sim 500$). Based on the above information, in order to unify all the correlations $(\mu/\mu_w)^{0.14}$ is added to correlations in [8,15,29] that did not originally include it. It also should be noticed that the exponent on Prandtl number is 0.333 for all correlations except for Focke's equation (0.5) [8], Talik's equation (0.4) [15], and Khan's equation (0.35) [36]. These three exponents are modified into 0.333. By simplifying in this way, the deviation from the new correlation to the original one is about 12.2–30.8% for Focke's equation, 4.7–11.1% for Talik's equation, and 1.2–3.2% for Khan's equation. Some analysis regarding the accuracy variation caused by those simplifications will be discussed later. It also should be pointed that there are other well-established empirical correlations in the open literature like Chisholm's equation [43] and Longo's equation [44]. Only correlations in [8,15,17,18,30,34,37] are selected since information of geometric parameters and definitions of dimensionless numbers are clearly given in those publications.

The comparison between our correlations and the correlations in [8,15,17,18,29,33,36] is shown in Fig. 9. The two main geometric parameters, enlargement factor ϕ (ratio of real/effective area to projected/nominal area) and corrugation profile aspect ratio γ, are given in the figure. As seen in Fig. 9(a), there is huge difference between different empirical equations at high herringbone angle. The difference is large as well at lower angles, as shown in Fig. 9 (b) and (c). From the results in Fig. 9 and the conclusions in the literature, the main reason for the large disagreement is the geometry variation. For example, corrugation profile aspect ratio γ and enlargement factor ϕ have a wide range: 0.5714–0.8269 and 1.16–1.29, even at the same herringbone angle. Consequently, the difference is very large. Although all correlations in Fig. 9 utilize projected area as heat transfer area, there is still difference between different projected areas. For example, one may use $L_1 \times W_1$, $L_2 \times W_1$, $L_1 \times W_2$, or even $L_2 \times W_2$ as projected area, as shown in Fig. 1.

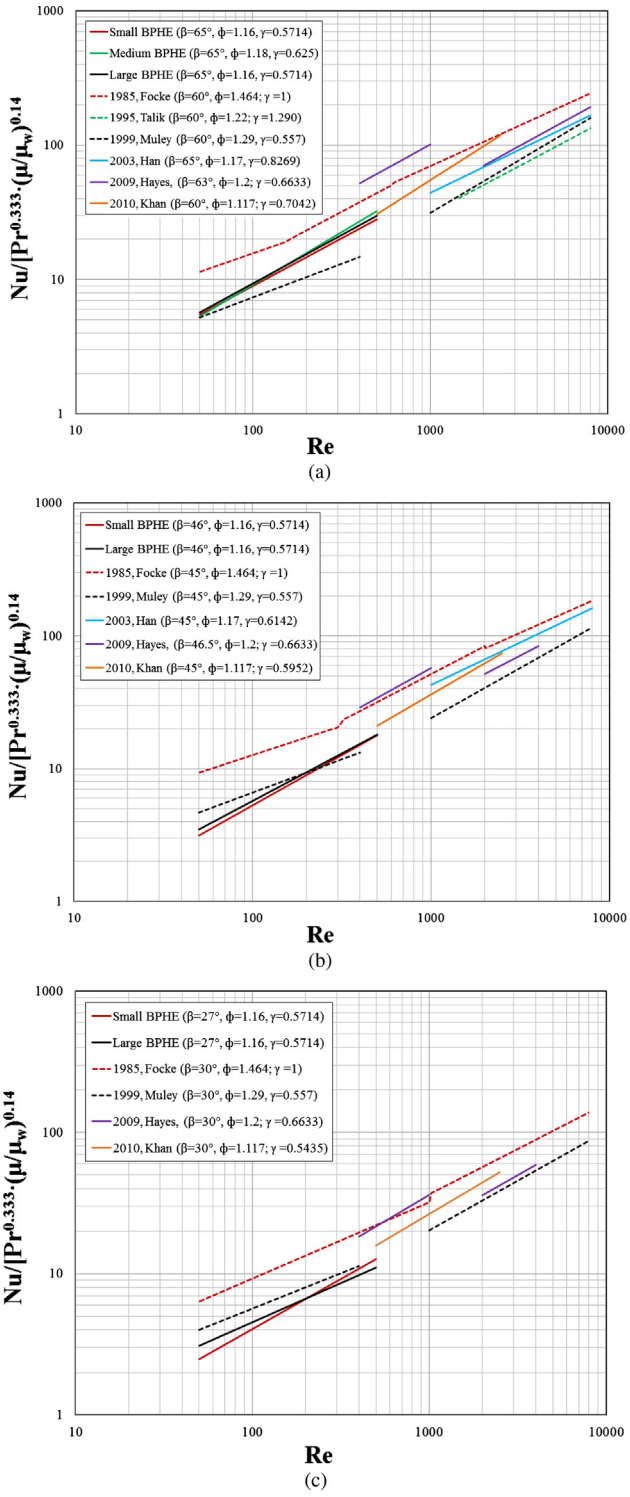

Fig. 9. The heat transfer performance in comparison with exsiting correlations: (a) high herringbone angle; (b) medium herringbone angle; (c) low herringbone angle.

It is more reasonable and applicable to propose some generalized correlations depending for a certain herringbone angle given that the herringbone angle is the most dominant factor that determines heat transfer performance. Then a more generalized correlation including herringbone angle effect is proposed. It should be noticed that three out of six equations Hayes et al. proposed in

[33] that uses dynalene/water mixture as working fluid are removed in the following generalization because they used the fluid to evaporate CO_2 thus the working temperature is much lower (−40 °C) than all other mentioned work.

At high herringbone angle (around 65°), the following correlation is given to predict heat transfer performance:

$$Nu = 0.5941 \cdot Re^{0.6103} \cdot Re^{\phi/60} \cdot Re^{\gamma/60} \cdot Pr^{1/3} \cdot \left(\frac{\mu}{\mu_w}\right)^{0.14} \quad (18)$$

The calculated heat transfer performance obtained by using Eq. (18) is compared to the real value as shown in Fig. 10. The deviation is within 50% due to the complex configuration inside plate heat exchangers. At medium herringbone angle (around 45°), the following correlation is given to predict heat transfer performance:

$$Nu = 0.5343 \cdot Re^{0.5903} \cdot Re^{\phi/45} \cdot Re^{\gamma/45} \cdot Pr^{1/3} \cdot \left(\frac{\mu}{\mu_w}\right)^{0.14} \quad (19)$$

The calculated heat transfer performance is compared to the real value as shown in Fig. 11. The deviation is within 50% as well because of the various heat exchangers. At low herringbone angle (around 30°), the following correlation is given to predict heat transfer performance:

$$Nu = 0.4139 \cdot Re^{0.5345} \cdot Re^{\phi/30} \cdot Re^{\gamma/30} \cdot Pr^{1/3} \cdot \left(\frac{\mu}{\mu_w}\right)^{0.14} \quad (20)$$

The calculated heat transfer performance is compared to the real value as shown in Fig. 12. The deviation is within 40% as there are less heat exchangers when herringbone angle is low.

Therefore, the *ACRC* correlation for Nusselt number is given as follows based on the three previous correlations:

$$Nu = \left(-1.342 \times 10^{-4} \cdot \beta^2 + 1.808 \times 10^{-2} \cdot \beta - 0.0075\right) \cdot Re^{(-7.956\times10^{-5}\cdot\beta^2+9.687\times10^{-3}\cdot\beta+0.3155)} \cdot Re^{\phi/\beta} \cdot Re^{\gamma/\beta} \cdot Pr^{1/3} \cdot \left(\frac{\mu}{\mu_w}\right)^{0.14}$$
$$50 \leqslant Re \leqslant 8000;\ 2 \leqslant Pr \leqslant 290 \quad (21)$$

Three geometric parameters: herringbone angle, enlargement factor, and corrugation profile aspect ratio, are directly correlated in the empirical equation. The correlation indicates that the single-phase heat transfer performance increases with the increase of Reynolds number, herringbone angle, enlargement factor, and corrugation profile aspect ratio, which is so far consistent with current findings. The generalized *ACRC* correlation includes 22 different plate heat exchangers, 25 various correlations from 1985 to 2015 with a wide range of geometric parameters and working conditions: $50 \leqslant Re \leqslant 8000$; $2 \leqslant Pr \leqslant 290$; $27° \leqslant \beta \leqslant 63°$; $1.16 \leqslant \phi \leqslant 1.464$; $0.557 \leqslant \gamma \leqslant 1.290$.

The comparison between the calculated values obtained by Eq. (21) and the real values in shown in Fig. 13. As shown in figure, the accuracy is about 50% due to the complex and various configurations of plate heat exchangers. It should be noticed that 95% data points are within 50% accuracy if the viscosity-variation correction factor effect and the exponent variation effect on Prandtl number are taken into consideration. Therefore, it can be concluded that the *ACRC* correlation has a comparably trustworthy accuracy on predicting PHE's heat transfer performance. More experimental work is in demand in order to propose more accurate empirical correlations and figure out state-of-the-art for plate heat

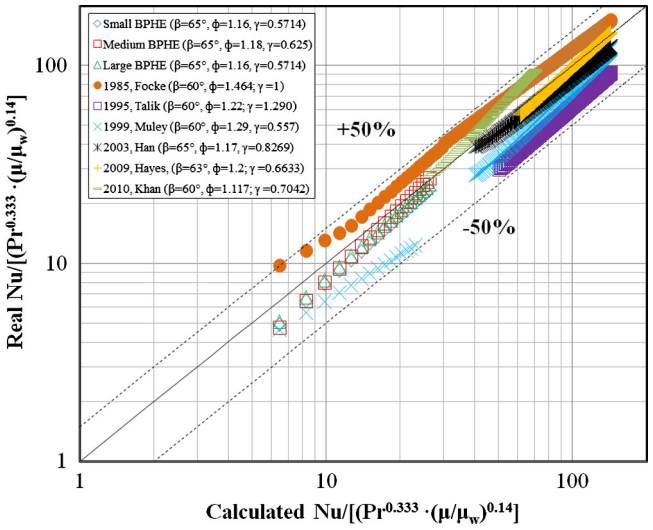

Fig. 10. The calculate heat transfer performance in comparison with the real heat transfer performance at high herringbone angle.

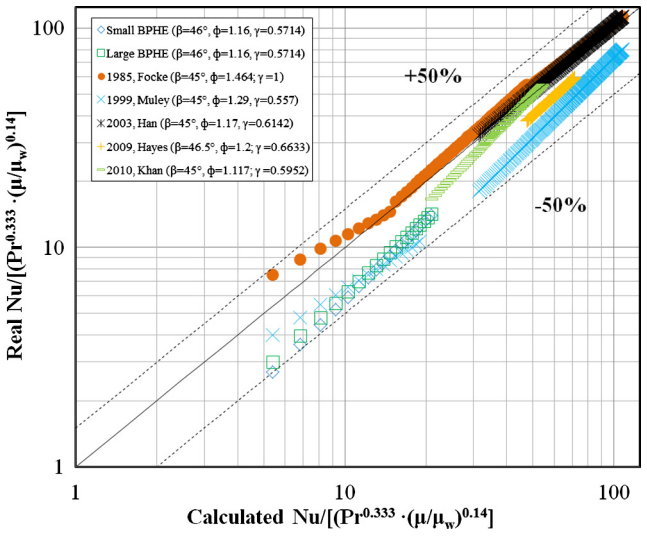

Fig. 11. The calculate heat transfer performance in comparison with the real heat transfer performance at medium herringbone angle.

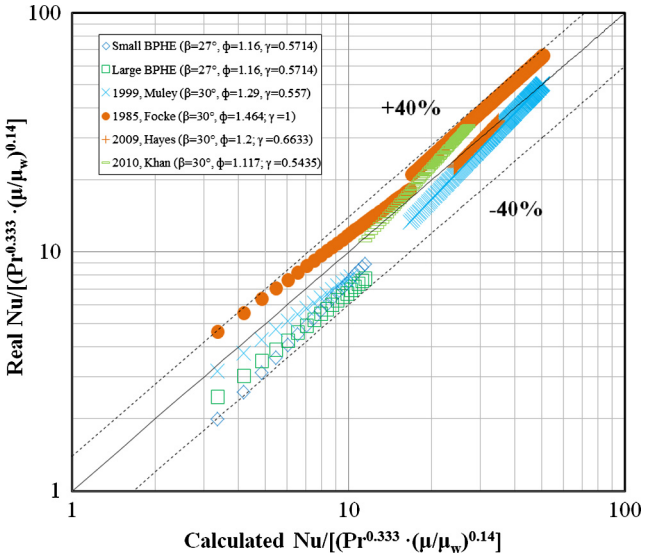

Fig. 12. The calculate heat transfer performance in comparison with the real heat transfer performance at low herringbone angle.

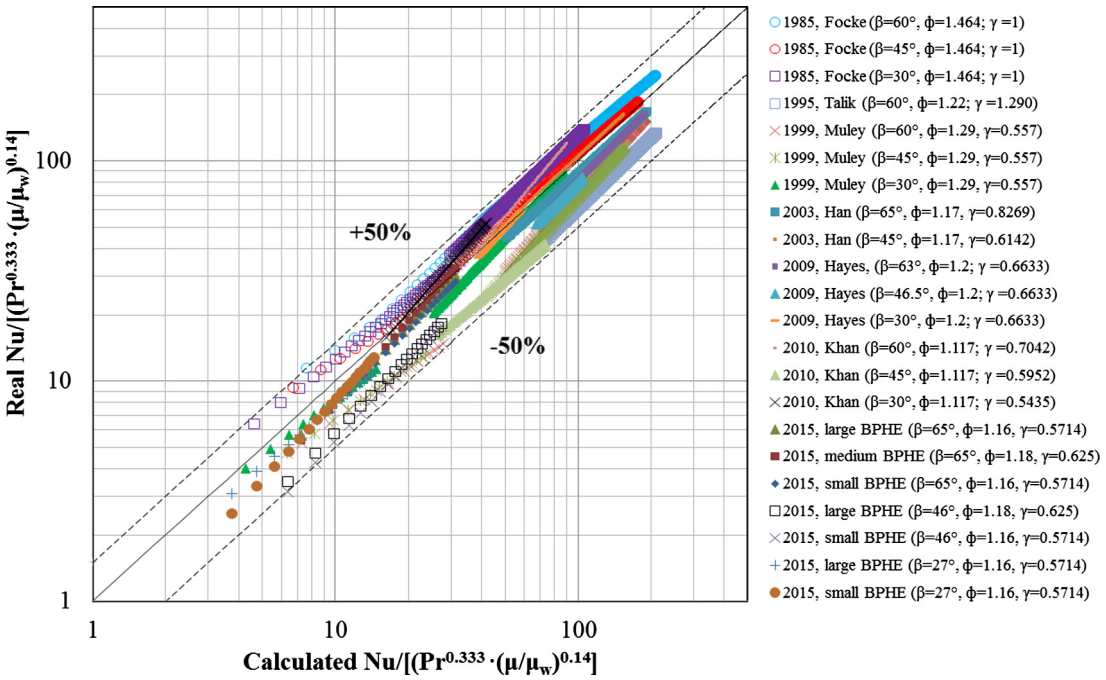

Fig. 13. The calculated heat transfer characteristics obtained by the *ACRC* correlation (21) versus real value.

exchangers. The generalization of pressure drop or friction characteristics will be given in the future since it is directly relevant with the real application.

3. Conclusions

In the present paper, the single-phase heat transfer of nine brazed plate heat exchangers for high Prandtl number fluid (EG/water mixture) with different geometric parameters is experimentally investigated. First, the specific heat transfer correlations for each BPHE are proposed using the modified Wilson plot. A general empirical correlation is proposed as well based on the experimental data. It is found that herringbone angle is the most influential factor. Generally, the single-phase heat transfer is enhanced with the increase of this angle. It is also found that geometric dimensions play a role on deciding heat transfer characteristics. But PHE with large/small dimensions do not necessarily lead to good/poor heat transfer. The geometric dimensions affect heat transfer in a collaborative way with herringbone angle. Second, the proposed correlations are compared with the current well-established correlations. It is found that there are great difference between our correlations and the existing correlations. The main reasons are from the following three aspects: the large range of geometric parameters, the wide range of dimensionless numbers, and the different definitions of projected/real heat transfer area. Third, the generalization for single-phase heat transfer of PHEs based on experimental data is given and the corresponding generalized correlation is proposed to calculate heat transfer performance. The *ACRC* correlation has the accuracy of 50% and it is applicable for a large range of PHEs. More experiments are in demand to propose more accurate correlation thus to design and optimize plate heat exchanger.

Acknowledgments

This work was proposed and conducted strictly at the University of Illinois, with funding provided by the Air Conditioning and Refrigeration Center (ACRC). The authors also acknowledge *Danfoss China* and support from *Danfoss North America* for providing the test BPHEs.

References

[1] K. Thulukkanam, Heat Exchanger Design Handbook, second ed., CRC Press, New York, 2013.
[2] Z.H. Ayub, Plate heat exchanger literature survey and new heat transfer and pressure drop correlations for refrigerant evaporators, Heat Transfer Eng. 24 (2003) 3–16.
[3] R.M. Manglik, Plate heat exchangers for process industry applications: enhanced thermal-hydraulic characteristics of chevron plates, process, enhanced and multiphase heat transfer, in: A.E. Bergles, R.M. Manglik, A.D. Kraus (Eds.), A Festschrift, Begell House, New York, 1996, pp. 267–276.
[4] L. Wang, B. Sunden, R.M. Manglik, Plate Heat Exchangers: Deign, Applications and Performance, first ed., WIT press, Billerica, 2007.
[5] H. Martin, Pressure drop and heat transfer in plate heat exchangers, in: Gesellschaft (Ed.), VDI Heat Atlas, Springer, New York, 2010, pp. 1515–1520.
[6] B.W. Jackson, R.A. Troupe, Laminar flow in a plate heat exchanger, Chem. Eng. Prog. 60 (1964) 65–67.
[7] K. Okada, M. Ono, T. Tomimura, T. Okuma, H. Konno, S. Ohtani, Design and heat transfer characteristics of a new plate heat exchanger, Heat Transf. Jpn. Res. 1 (1972) 90–95.
[8] W.W. Focke, J. Zachariades, I. Oliver, The effect of the corrugation inclination angle on the thermohydraulic performance of plate heat exchangers, Int. J. Heat Mass Transfer 28 (1985) 1469–1479.
[9] S.G. Kandlikar, R.K. Shah, Multipass plate heat exchangers-effectiveness-NTU results and guidelines for selecting pass arrangements, ASME J. Heat Transfer 111 (1989) 300–313.
[10] S.G. Kandlikar, R.K. Shah, Asymptotic effectiveness-NTU formulas for multipass plate heat exchangers, ASME J. Heat Transfer 111 (1989) 314–321.
[11] A.S. Wanniarachchi, U. Ratnam, B.E. Tilton, K. Dutta-Roy, Approximate correlations for chevron-type plate heat exchangers, in: Proceedings of the 30th National Heat Transfer Conference, Heat Transfer Division, New York, USA, 1995, pp. 145–151.
[12] H. Martin, A theoretical approach to predict the performance of chevron-type plate heat exchangers, Chem. Eng. Process. 35 (1996) 301–310.
[13] B. Thonon, R. Vidil, C. Marvillet, Recent research and developments in plate heat exchangers, J. Enhanc. Heat Transfer 2 (1995) 149–155.
[14] B. Thonon, Design method for plate evaporators and condensers, 1st International Conference on Process Intensification for the Chemical Industry, vol. 18, BHR Group Conference Series Publication, 1995, pp. 37–47.
[15] A.C. Talik, L.S. Fletcher, N.K. Anand, L.W. Swanson, Heat transfer and pressure drop characteristics of a plate heat exchanger, in: Proceedings of the ASME/JSME Thermal Engineering Conference, New York, USA, 1995, pp. 321–329.
[16] A.C. Talik, L.S. Fletcher, N.K. Anand, L.W. Swanson, Heat transfer and pressure drop characteristics of a plate heat exchanger using a propylene-glycol/water mixture as the working fluid, in: Proceedings of 30th National Heat Transfer Conference, New York, USA, 1995, pp. 83–88.

[17] A. Muley, R.M. Manglik, Experimental study of turbulent flow heat transfer and pressure drop in a plate heat exchanger with chevron plates, ASME J. Heat Transfer 121 (1999) 110–117.
[18] A. Muley, R.M. Manglik, H.M. Metwally, Enhanced heat transfer characteristics of viscous liquid flows in a chevron plate heat exchanger, ASME J. Heat Transfer 121 (1999) 1011–1017.
[19] M. Hessami, An experimental investigation of the performance of cross-corrugated plate heat exchangers, J. Enhanc. Heat Transfer 10 (2003) 379–393.
[20] J.A.W. Gut, R. Fernandes, J.M. Pinto, C.C. Tadini, Thermal model validation of plate heat exchangers with generalized configurations, Chem. Eng. Sci. 59 (2004) 4591–4600.
[21] B. Palm, J. Claesson, Plate heat exchangers: calculation methods for single- and two-phase flow, Heat Transfer Eng. 27 (2008) 88–98.
[22] N. Hayes, A. Jokar, Dynalene/water correlations to be used for condensation of CO_2 in brazed plate heat exchangers, ASHRAE Trans. 155 (2009) 599–616.
[23] D. Dovic, B. Palm, S. Svaic, Generalized correlations for predicting heat transfer and pressure drop in plate heat exchanger channels of arbitrary geometry, Int. J. Heat Mass Transfer 52 (2009) 4553–4563.
[24] A. Durmus, H. Benli, I. Kurtbas, H. Gul, Investigation of heat transfer and pressure drop in plate heat exchangers having different surface profiles, Int. J. Heat Mass Transfer 52 (2009) 1451–1457.
[25] T.S. Khan, M.S. Khan, M.C. Chyu, Z.H. Ayub, Experimental investigation of single phase convective heat transfer coefficient in a corrugated plate heat exchanger for multiple plate configurations, Appl. Therm. Eng. 30 (2010) 1058–1065.
[26] A.K. Tiwari, P. Gohsh, J. Sarkar, Heat transfer and pressure drop characteristics of CeO_2/water nanofluid in plate heat exchanger, Appl. Therm. Eng. 57 (2013) 24–32.
[27] O.P. Arsenyeva, L.L. Tovazhnyanskyy, P.O. Kapustenk, O.V. Demirskiy, Generalized semi-empirical correlation for heat transfer in channels of plate heat exchanger, Appl. Therm. Eng. 70 (2014) 1208–1215.
[28] Y.Y. Yan, T.F. Lin, Evaporation heat transfer and pressure drop of refrigerant R-134a in a plate heat exchanger, ASME J. Heat Transfer 121 (1999) 118–127.
[29] D.H. Han, K.J. Lee, Y.H. Kim, Experiments on the characteristics of evaporation of R410A in brazed plate heat exchangers with different geometric configurations, Appl. Therm. Eng. 23 (2003) 1209–1225.
[30] G.A. Longo, A. Gasparella, Heat transfer and pressure drop during HFC refrigerant vaporisation inside a brazed plate heat exchanger, Int. J. Heat Mass Transfer 50 (2007) 5194–5203.
[31] E. Djordjevic, S. Kabelac, Flow boiling of R134a and ammonia in a plate heat exchanger, Int. J. Heat Mass Transfer 51 (2008) 6235–6242.
[32] T.S. Khan, M.S. Khan, M.C. Chyu, Z.H. Ayub, J.A. Chattha, Review of heat transfer and pressure drop correlations for evaporation of fluid flow in plate heat exchangers, HVAC&R Res. 15 (2009) 169–188.
[33] N. Hayes, A. Jokar, Z.H. Ayub, Study of carbon dioxide condensation in chevron plates exchangers; heat transfer analysis, Int. J. Heat Mass Transfer 54 (2011) 1121–1131.
[34] N. Hayes, A. Jokar, Z.H. Ayub, Study of carbon dioxide condensation in chevron plate exchangers; pressure drop analysis, Int. J. Heat Mass Transfer 55 (2012) 2916–2925.
[35] H. Lee, S. Li, Y. Hwang, R. Radermacher, H.H. Chun, Experimental investigations on flow boiling heat transfer in plate heat exchanger at low mass flux condition, Appl. Therm. Eng. 61 (2013) 408–415.
[36] M.S. Khan, T.S. Khan, M.C. Chyu, Z.H. Ayub, Evaporation heat transfer and pressure drop of ammonia in a mixed configuration chevron plate heat exchanger, Int. J. Refrig. 41 (2014) 92–102.
[37] Y.G. Park, L.P. Liu, A.M. Jacobi, Rational approaches for combining redundant, independent measurements to minimize combined experimental uncertainty, Exp. Therm. Fluid Sci. 34 (2010) 720–724.
[38] J. Fernández-Seara, F.J. Uhía, J. Sieres, A. Campo, A general review of the Wilson plot method and its modifications to determine convection coefficients in heat exchanger devices, Appl. Therm. Eng. 27 (2007) 17–18.
[39] F.W. Dittus, L.M.K. Boelter, Heat transfer in automobile radiators of the tubular type, Univ. Cal. Publ. Eng. 2 (2) (1930) 443–461.
[40] D.P. Shah, Sekulic, Fundamentals of Heat Exchanger Design, first ed., Wiley, New York, 2003.
[41] A.J. Wheeler, A.R. Ganji, Introduction to Engineering Experimentation, second ed., Pearson Prentice hall, New Jersey, 2004.
[42] A.I. El. Sherbini, A. Joardar, A.M. Jacobi, Modified Wilson-plot technique for heat exchanger performance: strategies for minimizing uncertainty in data reduction, in: Proceeding of the 4th International Refrigeration and Air Conditioning Conference, Purdue, USA, 2004, pp. 1–8.
[43] D. Chisholm, A.S. Wanniarachchi, Maldistribution in single-pass mixed channel plate heat exchangers, in: Compact Heat Exchangers for Power and Process Industries, HTD-ASME, vol. 201, New York, 1992, pp. 95–99.
[44] G.A. Longo, A. Gasparella, Refrigerant R134a vaporization heat transfer and pressure drop inside a small brazed plate heat exchanger, Int. J. Refrig. 30 (2007) 821–830.